Journal of Chromatography A, 1218 (2011) 4179–4187

Contents lists available at ScienceDirect

Journal of Chromatography A

journal homepage: www.elsevier.com/locate/chroma

Sedimentation field flow fractionation and flow field flow fractionation as tools for studying the aging effects of WO_3 colloids for photoelectrochemical uses

Catia Contado [a,*], Roberto Argazzi [b]

[a] Department of Chemistry, University of Ferrara, via L. Borsari 46, I-44100 Ferrara, Italy
[b] Istituto per la Sintesi Organica e la Fotoreattività ISOF-CNR, c/o Department of Chemistry, University of Ferrara, via L. Borsari 46, I-44121 Ferrara, Italy

ARTICLE INFO

Article history:
Available online 3 December 2010

Keywords:
WO_3
Colloids
Photocatalytic films
Electrochemical characterization
Field flow fractionation

ABSTRACT

WO_3 colloidal suspensions obtained through a simple sol–gel procedure were subjected to a controlled temperature aging process whose time evolution in terms of particle mass and size distribution was followed by sedimentation field flow fractionation (SdFFF) and flow field flow fractionation (FlFFF). The experiments performed at a temperature of 60 °C showed that in a few hours the initially transparent sol of WO_3 particles, whose size was less than 25 nm, undergoes a progressive size increase allowing nanoparticles to reach a maximum equivalent spherical size of about 130 nm after 5 h. The observed shift in particle size distribution maxima (SdFFF), the broadening of the curves (FlFFF) and the SEM–TEM observations suggest a mixed mechanism of growth-aggregation of initial nanocrystals to form larger particles. The photoelectrochemical properties of thin WO_3 films obtained from the aged suspensions at regular intervals, were tested in a biased photoelectrocatalytic cell with 1 M H_2SO_4 under solar simulated irradiation. The current–voltage polarization curves recorded in the potential range 0–1.8 V (vs. SCE) showed a diminution of the maximum photocurrent from 3.7 mA cm^{-2} to 2.8 mA cm^{-2} with aging times of 1 h and 5 h, respectively. This loss of performance was mainly attributed to the reduction of the electroactive surface area of the sintered particles as suggested by the satisfactory linear correlation between the integrated photocurrent and the cyclic voltammetry cathodic wave area of the W(VI) → W(V) process measured in the dark.

1. Introduction

Tungsten trioxide (WO_3) is an indirect band gap semiconductor with interesting photoelectrochemical properties such as its reversible color change upon absorption of light and in response to an electrically induced change in oxidation state. WO_3 has potential applications for solar energy and electrochromic devices [1–3], besides being one of the best candidates for gas sensing [4]. WO_3 is also a novel purificatory ecomaterial suitable for application in energy renewal, energy storage and environmental cleanup. Considerable attention has been recently drawn to WO_3 thanks to its high efficiency in photocatalytic degradation of organic compounds, including a large fraction of environmental toxins [5]. WO_3 films can be used for the fabrication of smart windows, electronic displays, sunroofs, rear and side view mirrors [6]. Nanocrystalline WO_3 thin films can be also used as high performance photoanodes for water photoelectrolysis [7–10].

Numerous electrochemical and chemical techniques were used for the preparation of WO_3 thin films such as WO_3 electrodeposition from aqueous peroxytungstic acid solutions, potentiostatic anodization of W plates, reactive sputtering, plasma-enhanced chemical vapor deposition (PECVD), spray pyrolysis, pulsed spray pyrolysis, vacuum thermal evaporation of WO_3 powder, reactive sputtering of metallic tungsten and deposition through sol–gel procedure [11–12, and references therein].

Since the first cheap and easy sol–gel synthesis of electrochromic WO_3 in 1984 [13], where colloidal tungsten oxide was obtained via the condensation of tungstic acid in aqueous solutions, most of the methods have been optimized for the synthesis of nanometer particles, such as the production of microemulsions that contain surfactant, oil, water and sometimes co-surfactant [1].

Although the quality of the films is generally good, some WO_3 thin films may be amorphous or polycrystalline depending on colloid preparation conditions, deposition temperature and, in particular, post-deposition annealing treatments. Since the nanocrystalline materials exhibit different physical and chemical properties compared with conventional coarse-grained structures [1], in the last ten years, there has been an increasing interest in their study. Furthermore, since the current–voltage behavior of the photoanodes is strongly affected by the crystal size, the nanoparticle aggregation and the thickness of the photoactive layer, understanding and improvement of the film properties call

* Corresponding author. Tel.: +39 0532 455149; fax: +39 0532 240709.
E-mail address: Catia.Contado@unife.it (C. Contado).

0021-9673/$ – see front matter © 2010 Elsevier B.V. All rights reserved.
doi:10.1016/j.chroma.2010.11.061

for a better knowledge of their morphological and structural characteristics [14].

Different techniques can be used to obtain WO_3 particle size information and these are usually divided into separation and bulk techniques. The former group includes chromatographic, electrophoretic and field flow fractionation (FFF) techniques whereas advanced microscopy techniques, such as scanning electron microscopy (SEM), transmission electron microscopy (TEM), atomic force microscopy (AFM), and light scattering based techniques are found in the latter.

The microscopy techniques have the potential risk of modifying the aggregate structure during the handling or biasing aggregate orientation on a slide; the environmental scanning electron microscopy (ESEM) or wet scanning electron microscopy (WetSEM) can only overcome some limitations caused by sample preparation (e.g., drying) that could produce sample alteration or imaging artifacts. Although the techniques based on the static and dynamic light scattering principles [15,16] are powerful *in situ* characterization tools, able to rapidly provide accurate results they have only been developed for particle populations with a high level of monodispersity and size measurements are dependent on the knowledge of different physical properties that can be difficult to determine.

The advantages offered by the separation methods, especially by the FFF techniques [17], are mainly due to their non-disruptive nature: the colloids are separated according to their size or mass in a dispersed state (liquid phase) so that the derived particle size distributions (PSDs) should be more reliable than those obtained from bulk observations or under high vacuum conditions. Moreover, specific detectors, such as those based on light scattering, could be easily coupled on-line [18,19] in order to achieve a more complete description of the chemical–physical sample properties.

In this work, WO_3 thin films were prepared by coating conductive glass with a colloidal suspension of nano- and micro WO_3 particles achieved by a patented synthetic method [20], in which PEG-BAE and Triton X-100 were used as surfactants. This method, derived from [21], allows to create WO_3 nanoparticles of about 20–30 nm, whose size evolves spontaneously with time when the colloidal suspension is left to age. In a previous work, WO_3 colloids, prepared with the same procedure, were employed to make thin films used as photoanodes [22] without paying attention to the time elapsed from the colloid synthesis and the film preparation.

A controlled heating of the WO_3 colloidal precursor at constant temperature (40 and 60 °C) was carried out for 3 or 5 h in order to investigate the aging effects of the WO_3 suspension for the first time in this study. After fixed intervals, the suspension aliquots were withdrawn to make the photoanodes. At the same time, a portion of the collected aliquots was properly diluted and analyzed through sedimentation FFF (SdFFF) and flow FFF (FlFFF) in order to obtain suspension particle size information [17,23,24] during the colloid growth. The SdFFF was chosen because it provides direct and absolute information on the effective mass of particles or aggregates whereas the FlFFF was selected because it separates particles according to their diffusion coefficient which can be related to their hydrodynamic diameter. The size results were supported by SEM and TEM observations.

The electrochemical and photoelectrochemical properties of the photoanodes were measured through current–voltage (JV) polarization curves and linear sweep cyclic voltammograms (CV).

2. Experimental

2.1. Reagents

The following chemicals were used, as received, for the preparation of WO_3 colloids and films: sodium tungstate dihydrate $Na_2WO_4{\cdot}2H_2O$ (Riedel de Haën), hydrochloric acid 37% (Sigma–Aldrich), oxalic acid dihydrate (Fluka), polyethyleneglycol bisphenol A epichlorydrin copolymer 15,000–20,000 Da (PEG-BAE, Sigma), Triton X-100 (Fluka) and sulphuric acid 95–97% (Sigma–Aldrich).

Polystyrene standard samples: PS nanosphere with nominal diameter of 46 nm ± 2.0 nm (Duke Scientific Co., Palo Alto, CA, USA) and 25 mg mL^{-1} Polystyrene Nanosphere (PPs-0.1, G.Kisker GbR Produkte f.d.Biotechnologie, Steinfurt, Germany) with nominal diameter of 96 nm; the commercial suspensions were diluted in the carrier solution prior to their use to check the FFF instruments.

Ultrapure deionized water (18 MΩ cm) obtained from the MilliQ Water purification system (Milli-Q system, Waters Corp., Milford, MA, USA), was used throughout the experiments.

The transparent conductive glass substrate used in the preparation of photoelectrodes was Fluorine doped Tin Oxide (FTO), TEC 8 8 Ω/□ from Hartford Glass.

Isopore™ membrane filters (VCTP, size pore 0.1 μm, Millipore) were used for the SEM observations.

2.2. Preparation of WO_3 colloids

In a typical preparation, 2.5 g of $Na_2WO_4{\cdot}2H_2O$ were dissolved in 100 mL of ultrapure deionized water in a 250 mL Erlenmeyer flask. 20 mL of concentrated HCl were rapidly added, to this solution, under magnetic stirring, by means of a 25 mL burette. The resulting turbid yellow suspension of tungstic acid was poured into a 100 mL centrifuge tube and the collected gel was thoroughly washed three times with 30 mL portions of pure water. The wet gel (typically about 11 g) was then peptized in a solution of 2 g of oxalic acid dihydrate (Mw = 126.1 g mol^{-1}) dissolved into 5 mL deionized water and maintained at 60 °C on a hot plate and its final concentration was about 1.5 M. The resulting transparent colloidal suspension was added with 20% of its weight of PEG-BAE (~3.6 g) at room temperature. Nine drops of Triton X-100 from a pasteur pipette ~0.18 mL) were finally added to the viscous suspension [20].

Controlled aging of the WO_3 suspension was accomplished in a 10 mL glass vial suspended in an ethylene glycol bath, heated continuously for 5 h, under vigorous stirring. The heating bath was brought to the desired temperature by means of an IKA RCT basic hot plate and maintained at 40 or 60 °C (±1 °C) with an IKA ETS-D4 electronic contact thermometer.

2.3. Preparation of WO_3 films

WO_3 photoelectrodes were prepared by spreading (scotch tape method) the colloidal precursor with a finely grounded edge glass slide onto FTO substrates previously cleaned and rinsed with deionized water and ethanol and finally dried at room temperature. A typical photoelectrode size was 4 cm × 2 cm with a 2.5 cm × 1.4 cm WO_3 coated area and 1.5 cm on top for electric contact.

The resulting films were dried in air at approximately 100 °C before firing at 550 °C in air for 30 min. After sintering, the photoelectrodes were immersed for 1 h in 1 M H_2SO_4, rinsed with plenty of deionized water, dried under a warm airflow and then fired again at 550 °C for another 30 min.

2.4. Sedimentation FFF equipment

The sedimentation FFF system Model S-101 particles/colloid fractionator (Postnova Analytics, Landsberg/Lech, Germany) was employed and its description is reported in detail in Refs. [25,26].

The carrier solution was Triton X-100 0.1% (v/v); the volumetric flow-rate was set at Q = 2.00 mL min^{-1} and measured during each run. The SdFFF rotations set to perform the fractionations,

Table 1
SdFFF power program field decay parameters. Decay law: $G = G_0((t_1 - t_a)/(t - t_a))^p$, $p = 8$.

Program	Initial RPM	Applied field G (gravities)	Relaxation time (min)	t_1 (min)	t_a (min)	Final RPM	Hold RPM
A	2000	674	5	10	−80	20	20
B	450	34	5	10	−80	20	20

along with the correspondent generated fields [27], are reported in Table 1. After injection, the carrier was stopped for 5 min (relaxation period) to allow the sample to equilibrate under the applied field. The SdFFF instrument was controlled by the SPIN 1409 program, which also acquired the fractograms; the registered data were processed by FFF ANALYSIS software to convert the retention times directly in diameters of the equivalent sphere (d_s); both programs were Windows compatible provided by Postnova Analytics (Germany) along with the instrument.

All fractionations were performed at room temperature (26 °C room conditioned).

2.5. Flow FFF system

The model F-1000 symmetric FlFFF channel (Postnova Analytics, Salt Lake City, UT, USA) was used to perform the colloid separations and the system was extensively described in previous papers [28,29]. The samples were injected through an 50 μL injection loop mounted on a Rheodyne 7725i sample valve (Rheodyne LLC, Rohnert Park, CA, USA); the regenerated cellulose (RC) membrane had a nominal cut-off of 10 kDa (UC010 T) (Microdyn-Nadir GmbH -Wiesbaden, Germany). The experimental channel thickness ($w = 0.0186$ cm) was computed from the analyses carried out on PS standards. The carrier solution was Triton X-100 0.1% (v/v). The volumetric flow-rates, longitudinal Q_L and cross Q_c respectively, were specific for each separation; Table 2 summarizes their values for the reported experiments.

The outlet tube from the FlFFF channel was connected to the UV detector Intelligent UV/Vis detector Jasco 875-UV (JASCO Europe s.r.l., Cremella (LC), Italy) with wavelength set at 254 nm.

The Q_L was stopped for 3 min (relaxation time) in order to equilibrate the samples with the applied field Q_c.

The FlFFF fractograms were converted to particle size distributions (PSDs) using a software developed in 1990 at the FFF Research Center (University of Utah, Salt Lake City, UT, USA).

2.6. Electrochemical and photoelectrochemical measurements

The electrochemical characterization of WO_3 films was performed using an a EcoChemie Autolab PGSTAT302N potentiostat. The irradiation of WO_3 photoelectrodes was carried out through an Abet Technologies LS-150-Xe solar simulator, provided with a AM1.5G filter, whose output was measured through a Newport 1918c optical power meter equipped with a 818P-015-18 thermopile detector. JV polarization curves and linear sweep cyclic voltammograms were recorded in 1 M H_2SO_4 in a three compartment cell, made of Pyrex glass, using a saturated calomel electrode as a reference and a coiled platinum wire as a counter electrode. The reference and counter electrodes were both separated from the central compartment, accommodating the working photoelectrode, by sintered glass frits. The cell was placed at a distance from the solar simulator chosen in such a way that the optical power density on the photoelectrode surface was within the range of 0.2–0.3 W cm^{-2}.

Table 2
Volumetric flow-rates applied during the FlFFF analyses.

Time – series at 60°	Q_L (mL min^{-1})	Q_c (mL min^{-1})	Q_c/Q_L
0 h	0.505 ± 0.001	0.474 ± 0.003	0.94
1 h	0.469 ± 0.019	0.436 ± 0.029	0.93
2 h	0.498 ± 0.011	0.457 ± 0.014	0.93
3 h	0.505 ± 0.005	0.471 ± 0.035	0.93
4 h	0.486 ± 0.012	0.453 ± 0.012	0.93
5 h	0.500 ± 0.008	0.469 ± 0.006	0.94

2.7. UV–Vis absorption spectroscopy

UV–Vis absorption and diffuse reflectance spectra of the deposited films were recorded with a Jasco V570 UV–Vis-NIR spectrophotometer equipped with a ISN-470 integrating sphere accessory. The spectral bandwidth was 2 nm for all measurements.

2.8. Other equipments

The vortex-Genie 2 mixer was purchased from Sigma–Aldrich. The microson ultrasonic cell disruptor (Model XL2000, Misonix, Farmingdale, NY) with a 0.48 cm diameter microtip probe was used at 50% of the output power (output power 50 W).

The scanning electron microscope (SEM) ZEISS EVO 40 was used to observe aliquots of the WO_3 colloids collected during the aging procedure by filtering the suspensions on Isopore™ membranes and the WO_3 films, in both cases glued on aluminum stubs using double-sided sticky tape (TAAB Laboratories Equipment, Ltd., Aldermaston, Berkshire, UK). The accelerating voltage was 20,000 kV.

The transmission electron microscope (TEM) (Hitachi H-800) was used to evaluate both size and morphology of the nanoparticles. Usually, a drop of the sample suspension was deposed on a copper grid (mesh 150) and let to dry at room temperature (25 °C).

3. Results and discussion

In order to investigate the effects of the WO_3 grain size on the photoelectrochemical performance of the films, the procedure to prepare the WO_3 colloidal suspension [20] was modified, thus accelerating the spontaneous particle growth which usually occurs in a few hours at room temperature, by heating the WO_3 colloidal suspension at 40 or 60 °C, under controlled conditions (see Section 2). Several series of photoanodes were made by sampling the suspensions after fixed intervals from the vial where the aging process was conducted and controlled. The aliquots were used “as is” to make the films and diluted 1:20 with deionized water in order to obtain their PSD through the FFF analyses. Before being injected into the SdFFF and FlFFF channels, all the diluted aliquots were always vigorously stirred for about 1 min with the vortex.

The FFF separations of the WO_3 colloids were carried out in a 0.1% (v/v) solution of Triton X-100 in order to maintain a continuity in the chemical composition of the media in which the WO_3 particles were dispersed and since the pH of this solution (pH = 5.97 ± 0.16 at 26 °C) does not allow the dissolution of the WO_3 colloid during the analysis [30]. The weakly acidic pH condition is also likely to allow a negative surface charge of the WO_3 colloid, which should minimize the interactions between the FlFFF membrane and the particles [30].

Some aliquots were analyzed 3 or 4 times to test the repeatability of the FFF results since the mass and size information were mainly derived from the fractograms; in all cases the results were

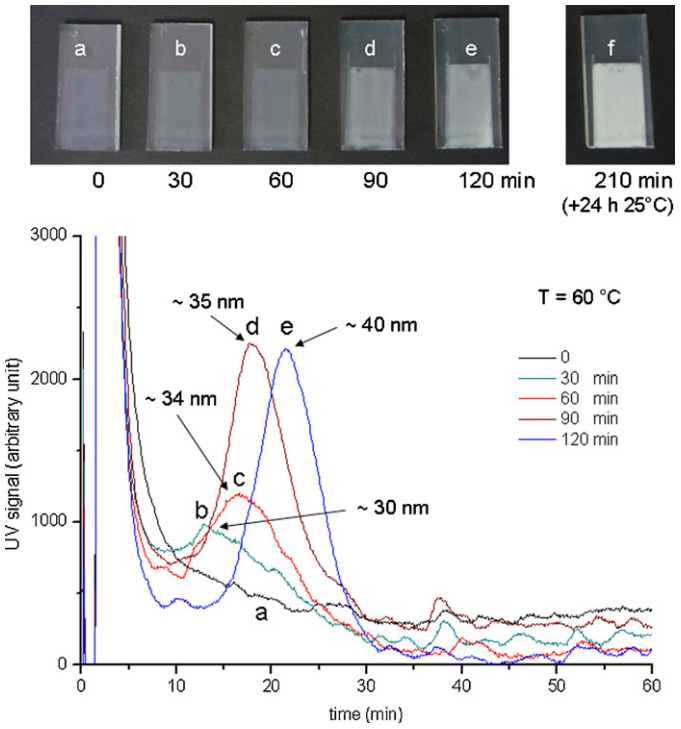

Fig. 1. SdFFF fractograms obtained from the WO_3 colloid aliquots sampled every 30 min from the suspension treated at 60 °C. Separation conditions: applied field = A, Table 1, UV range 0.002; flow rate 2.0 mL min^{-1}, carrier: Triton X-100 0.1% (v/v). On the top, photographs of the photoanodes obtained from the WO_3 aliquots.

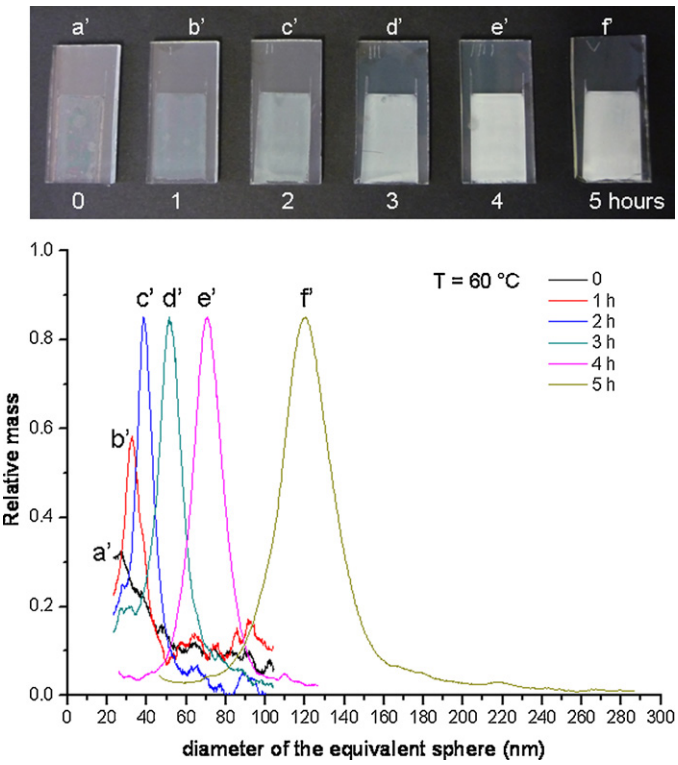

Fig. 2. PSDs sequence derived from the fractograms obtained from the WO_3 colloid aliquots sampled every hour from the suspension treated at 60 °C. Separation conditions: applied field for the aliquots a′–e′ = A, aliquot "f" B (Table 1), UV range 0.002; flow rate 2.0 mL min^{-1}, carrier: Triton X-100 0.1% (v/v). On the top, photograph of the photoanodes correspondent to the six WO_3 aliquots.

equivalents so that the figures used in this work usually report only one run.

The first set of photoanodes was prepared by using four aliquots of a WO_3 colloidal suspension aged at 40 °C and collected after 2, 4 and 5 h (see Supplementary material §1 for discussion).

From these first experiments, it was deduced that the WO_3 suspension thermal treatment at 40 °C did not affect the colloidal growth, even if some indications about the formation of larger particles was drawn. A higher temperature (60 °C) was chosen in order to accelerate the growing process, and the results are discussed in the following section.

3.1. Aging of the WO_3 suspension at 60 °C

3.1.1. SdFFF size characterization

Fig. 1 reports the SdFFF fractograms of the first series of five aliquots aged at 60 °C and sampled every 30 min. The WO_3 colloidal suspension, initially clear and transparent, became lightly turbid after 15 min and this change gradually increased with time; after 2 h it turned into a yellowish dense and creamy suspension (see Fig. S3, Supplementary material). The photograph of the films, which is on the top of the figure, is reported to show the increasing opacity of the photoanodes; the last anode was achieved by using an aliquot collected after 3 h:30 min of thermal treatment and left for 24 h at 25 °C.

The fractogram related to the first aliquot (t = 0 min) does not present any peak but the profile achieved by the aliquot taken after 30 min presents a small peak at about 15 min which correspond to an equivalent spherical particle diameter d_s of 30 nm, automatically computed by the Analysis program, if a bulk density of 7.2 g mL^{-1} is assumed for the WO_3 [22,31]. Later on, the fractograms obtained by the successive aliquots show some peaks, whose position gradually shifts towards higher retention times with a mass increment ($d_s \sim 40$ nm). It is important to note how these particles are slowly formed with time; the fractograms of the aliquots "c" and "d" indeed only differ in the peak area but not for the retention time and later on the particle mass gradually increases (aliquot "e"). Moreover, it is worth noting that also in this series, the void time peak is larger than that one registered for the "blank" solution (not reported in this figure, see Supplementary material for a comment of it), meaning that the suspension, even if treated at 60 °C should still contain a portion of smaller particles which are not fractionated.

In order to verify the reproducibility of these results, and hold a broader spectrum of opinions about the mass changes occurring during a 5 h range other experiments were repeated by keeping the same heating conditions (60 °C). Fig. 2 reports the PSDs, expressed as d_s, derived by the WO_3 colloidal suspension, sampled every 60 min and the obtained photoanodes are shown on the top of it.

The signal corresponding to the void peak was omitted to simplify the graph. The colloidal suspension was initially transparent (t = 0 min) but after 15 min became turbid and after 5 h it was yellow and very dense. A qualitative image of the suspension increased turbidity over time can be seen in the picture of the diluted aliquots taken from the suspension during the heating treatment and reported in Fig. S6, Supplementary material. The average particle sizes of the equivalent sphere measured by SdFFF gradually increased from 25 to 130 nm. Although quantitative measurements were not carried out, it can be easily deduced through an observation of the area subtended by the peaks that the amount of large particles formed as a result of the heating treatment increase with time.

3.1.2. SEM and TEM observations

In order to obtain information about the shape of the WO_3 colloidal particles, 50 μL of the diluted aliquots injected in the SdFFF were further diluted to 3 mL with deionized water, vigorously

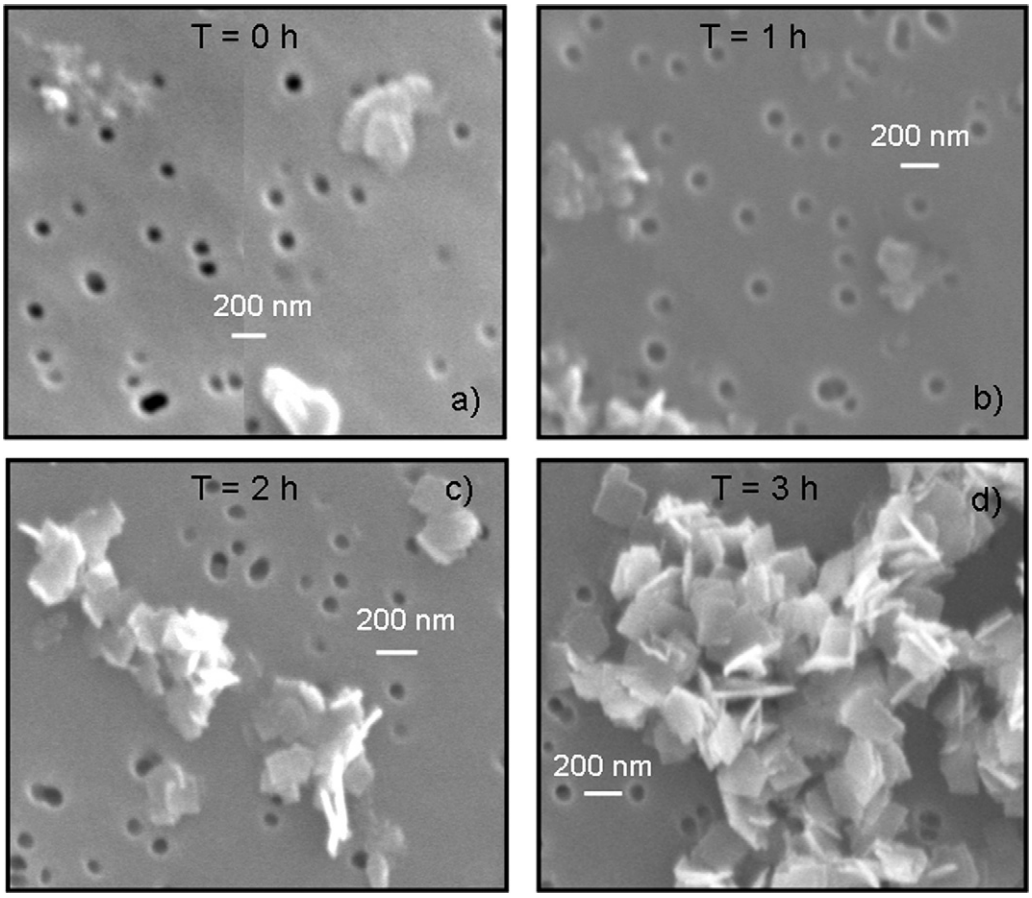

Fig. 3. SEM photographs taken on the WO_3 colloid aliquots sampled every hour from the suspension treated at 60 °C. (a) Aliquot at $t = 0$, 64.54 k magnification; (b) aliquot at $t = 1$ h, 72.28 k magnification; (c) aliquot at $t = 2$ h, 43.88 k magnification; (d) aliquot at 3 h, 43.88 k magnification.

mixed, filtered through a 100 nm membrane and observed by SEM, as shown in Fig. 3. The membrane pore size determines the loss of particles smaller than 100 nm, but a substantial amount of them was still observable in the first aliquot because of the large number of such particles initially present. Picture (a) shows the colloidal suspension before the heating treatment. Some particles retained by the filter are smaller than 50 nm, although some of them look as clusters or small agglomerate smaller than 300 nm. Picture (b) shows the aliquot after 1 h of heating: the particles smaller than 50 nm are still present and easily recognizable but their tendency to be distributed in larger clusters is increased compared with the initial condition. As time goes by, the amount of retained small particle decreases while the amount of well-defined square plates whose larger dimensions are about 150–250 nm increases (picture c). These plates are very thin, as it might be deduced by observing those particles which lie perpendicular to the filter. After 3 h of aging at 60° (d) only aggregates of square plate particles are visible. Although no particularly significant differences in the single particle size were detected, there was an increased tendency to form clusters where the plates overlap with the side of their larger dimensions.

This feature was also confirmed by the aliquots withdrawn after 4 and 5 h in which the single crystals seem to reach a limiting size of 300 nm, beyond which the aggregation process becomes more effective than the particle growth [32]. The increased amount of large plates can only be explained by a slow dissolution of the initially small particles in favour of the new crystalline particles.

Fig. 4 shows some TEM pictures of the aliquot withdrawn after 3 h of heating treatment; a drop of the diluted sample used for the SdFFF analysis was deposited on the copper grid. Picture (a) clearly shows an extended aggregate of square plates and several rounded particles smaller than 30 nm, which were not visible in the SEM picture because they passed through the filters. Pictures (b) and (c) highlight the typically regular shape of a crystalline material.

The SEM and TEM images show the single WO_3 particles as small square crystals of 150–300 nm diagonal (d_p) and a slight thickness t_p, i.e., particles with a high aspect ratio, *a.r.*, defined as:

$$a.r. = \frac{d_p}{t_p} \tag{1}$$

The microscopy observations validate the assumption that the sizes measured through SdFFF should only be expressed in terms of equivalent spherical diameter (d_s), especially for the analyses performed on the aliquots taken after 1 h of aging.

By assuming spherical and square-base parallelepiped particles of equal volume (mass) and a constant aspect ratio for all particles, the d_s can be related to the diagonal of the squares d_p simply considering geometrical factors, i.e. such as

$$d_s = \left(\sqrt[3]{\frac{3}{\pi \times a.r.}} \right) d_p = const \times d_p \tag{2}$$

Aspect ratios of 15–30 for the planar structure were reported in a recent paper [33]. By assuming that these values also hold true for these particles, the d_s computed by the SdFFF could be related to the observed d_p (see Table 3).

In order to confirm the d_p size distribution seen through SEM/TEM the WO_3 aliquots were also analyzed through FlFFF, which is known to give dimensional information expressed as hydrodynamic sizes d_h, close to the d_p values.

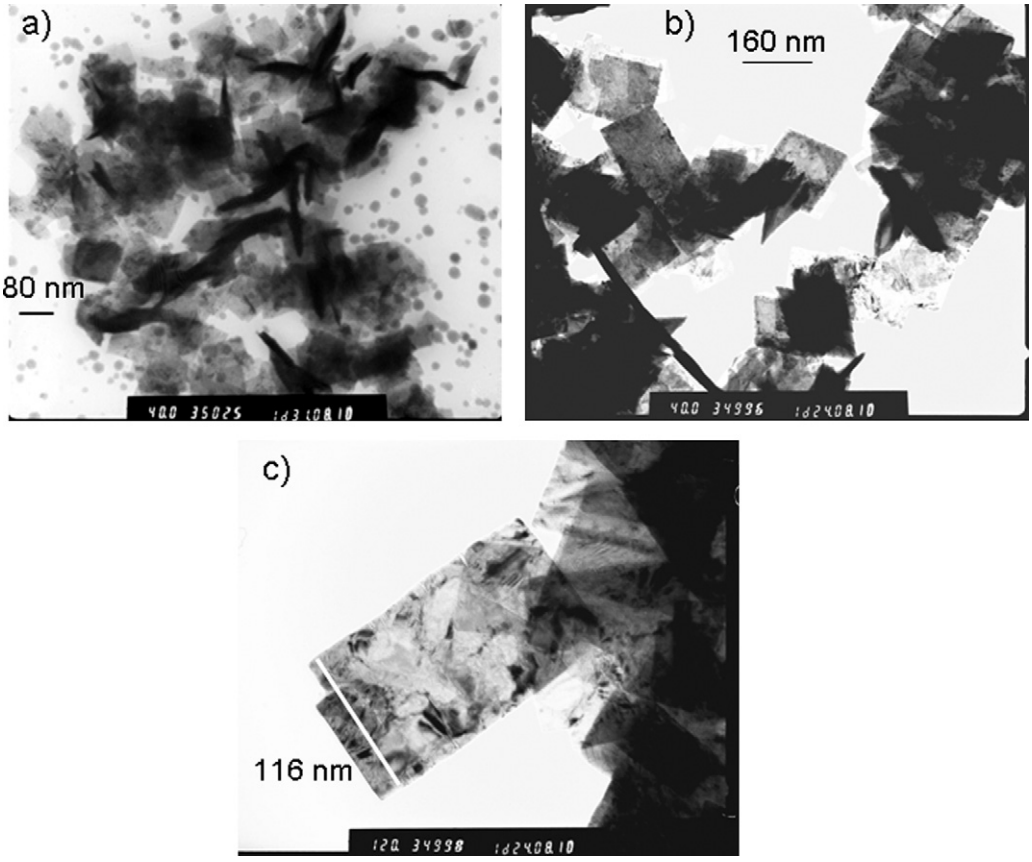

Fig. 4. TEM photographs taken on the WO_3 colloid aliquot sampled after 3 h of heating treatment at 60 °C. (a and b) 40 k magnification; (c) 120 k magnification.

3.1.3. FlFFF size characterization

Fig. 5a reports the FlFFF particle size distributions of the same six WO_3 aliquots described in Fig. 2. The elution profiles of the aliquots "a′" and "f′" are reported on the top of the figure (plot b). The fractograms allow to highlight (i) the shift of a first peak from the void time, (ii) the increased intensity of the broad signal between 15 and 60 min and (iii) the increased signal intensity of the post-analysis peaks, exiting when the cross-flow is stopped.

The PSDs present a first peak which initially overlapped completely with the void peak, due to particles of hydrodynamic size smaller than 50 nm. The rectangular zone in light gray, emphasizes that these data should be interpreted with caution, since the resolution chosen for these analyses (see Table 2) purposely neglects both the smallest particles whose information can be easily found in a variety of literature [21,22], as well as the largest ones, since the SEM and TEM observations demonstrated they are due to particle aggregates. The most interesting part of the PSDs is the signal spanning between 75 and 300 nm. The particles contained in all six aliquots are within this size range, although the first two aliquots "a′" and "b′" gave a weaker signal compared to the other four ("c′"–"f′"). The amount of particles with these sizes corresponding quite well to those observed through SEM and TEM, seems to be constant after the first hour of heating treatment, as if the growth process leads to a quasi-steady state, where the smallest particles disappear to form larger particles which, in turn, do form aggregates.

Moreover, the fractograms (plot b), prove that the number of aggregates significantly increases with the aging time (see peaks when the cross-flow is released).

The apparent contradiction of the FlFFF data with the SdFFF results presented in this section can be explained by looking at the data reported in Table 3, which summarizes the correspondence of the d_p values which can be best described by the d_h, and the d_s values. The first column reports the most probable *a.r.* values [33], from which the d_s are computed; a d_s 70 nm corresponds to particles with a d_p of 200 and an *a.r.* of 20.

It can therefore be deduced that the SdFFF is able to highlight the most likely mass, which may not correspond to a single size, especially for this type of sample where small aggregates of small particles may have the same mass as that of a single large particle.

Table 3
Correspondence between the sizes d_p and d_h measured through SEM, TEM and FlFFF and the equivalent spherical size d_s achievable through SdFFF.

a.r.	$d_p \approx d_h$ →	50 nm	100 nm	150 nm	200 nm	300 nm
10	d_s (nm)	22	44	66	87	130
15	d_s (nm)	19	38	58	76	114
20	d_s (nm)	18	35	52	70	104
30	d_s (nm)	15	31	46	61	91

3.2. Optical properties

The formation of particles of an increasingly larger mean diameter during the controlled temperature aging process, is responsible for the progressive increase in turbidity and the yellow color which were found to occur to the WO_3 suspensions. Consequently, the degree of opacity shown by the films made at regular intervals from the aging suspensions increases, as proven by the diffuse reflectance spectra shown in Fig. 6 related to the series of photoelectrodes (see Fig. 2) prepared as described above, at 1 h time periods. The curves are uniformly spaced along the visible part of the spectrum where WO_3 does not absorb and in this region are due to light scattering from the particles which constitute the films.

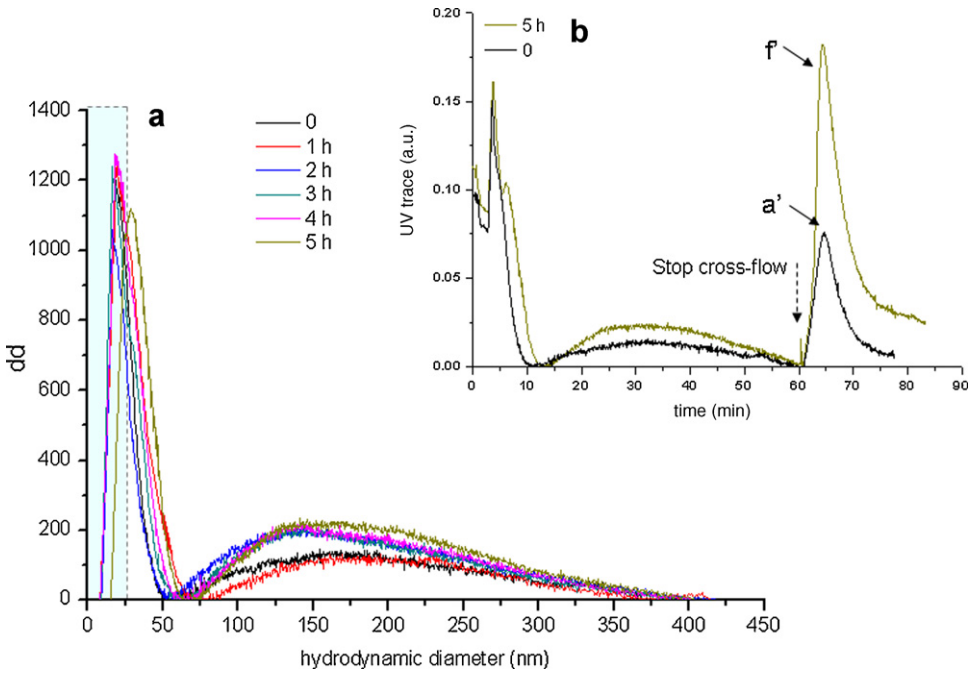

Fig. 5. (a) FlFFF PSDs of the WO_3 colloid aliquots sampled every hour from the suspension treated at 60 °C. (b) FlFFF fractograms of the aliquots "a′" (t = 0) and "f′" (t = 5 h). Separation conditions reported in Table 2; carrier: Triton X-100 0.1% (v/v).

Below 450 nm the band gap excitation of WO_3 is responsible for the strong featureless absorption (dashed line, on the left) reported in Fig. 6 (right scale) for the film obtained after 1 h of aging at 60 °C. The cutoff wavelength of the conductive glass substrate is about 350 nm.

3.3. Photoelectrochemical characterization

The photoelectrochemical properties of WO_3 films were tested recording J–V polarization curves in 1 M H_2SO_4, under solar simulated irradiation, in the potential range 0–1.8 V vs. SCE (Fig. 7). The photocurrent observed in these photoelectrolysis experiments under a voltage sweep at 20 mV s^{-1} and an optical power density of 0.24 W cm^{-2} is due to water splitting in which oxygen is evolved at the WO_3 surface as a consequence of oxidation of water molecules carried out by photogenerated holes left in the valence band of the irradiated semiconductor, while hydrogen is formed at the Pt electrode owing to the reduction of protons by electrons in the conduction band transferred to the counter electrode under the applied voltage bias. The photocurrent onset at 350 mV vs. SCE was the same for all curves which refer to a series of photoelectrodes obtained at 1 h time intervals aging a WO_3 suspension at 60 °C. The maximum photocurrent density of 3.7 mA cm^{-2} was reached with the first sample (1 h at 60 °C) and a uniform decrease was observed for the subsequent samples along with a progressive linearization of the curves. This behavior can be rationalized assuming that during the aging process larger WO_3 particles are successively formed and once they are deposited on a substrate and sintered at 550 °C

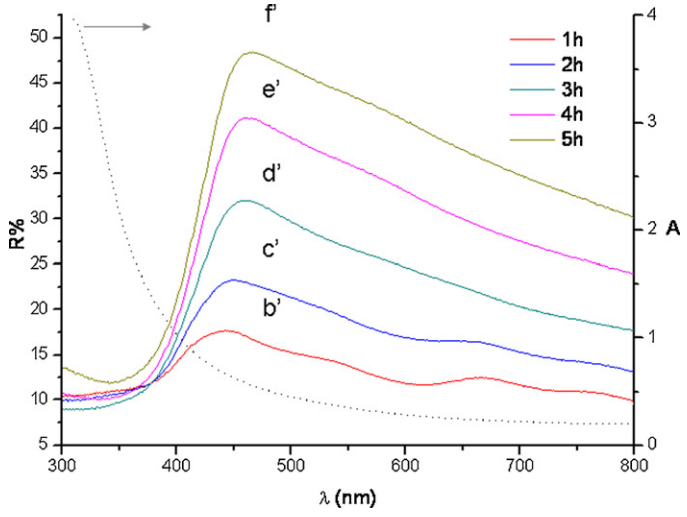

Fig. 6. Diffuse reflectance spectra (left scale) of WO_3 films prepared at 1 h time intervals from a colloid precursor aged at 60 °C (aliquots a′–e′ of Fig. 2). Absorption spectrum (right scale) of a transparent WO_3 film obtained after 1 h of aging (solid gray line).

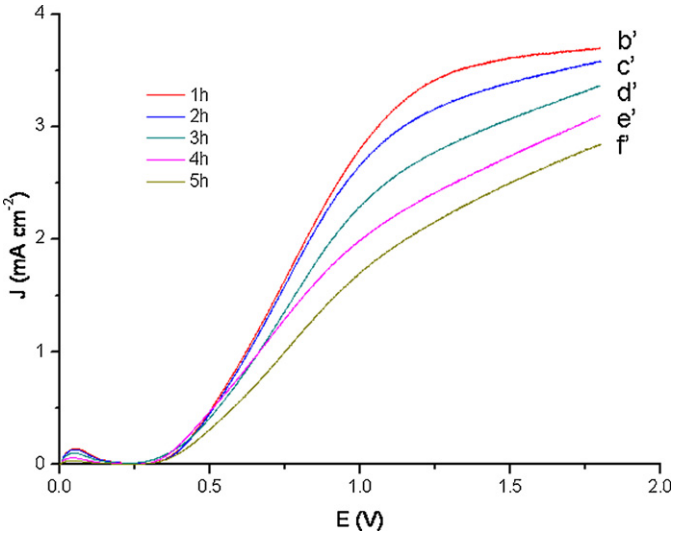

Fig. 7. J–V curves in 1 M H_2SO_4 under solar simulated irradiation (0.24 W cm^{-2}) of a series of WO_3 photoelectrodes prepared at 1 h intervals from a precursor suspension aged at 60 °C (aliquots a′–e′ of Fig. 3). Potential values are referred to SCE electrode.

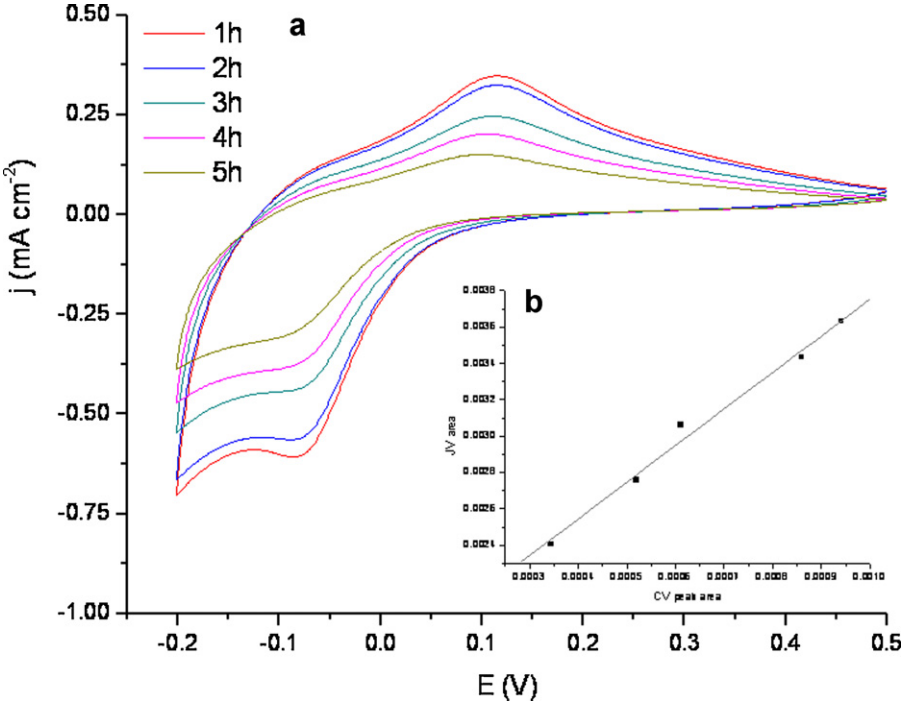

Fig. 8. (a) Cyclic voltammograms in 1 M H_2SO_4 of the W^{VI}/W^{V} process recorded in the dark for a series of photoelectrodes prepared at 1 h intervals from a precursor suspension aged at 60 °C (aliquots a′–e′ of Fig. 2). (b) Correlation between the CV cathodic wave area and the JV integrated curve area for a series of WO_3 photoelectrodes prepared at 1 h intervals from a precursor suspension aged at 60 °C. $JV_{area} = (6.1 \pm 0.3)10^{-3} + (2.01 \pm 0.13)CV_{area}$; $R^2 = 0.988$.

a coating of interconnected particles of less total surface area is obtained. This could cause a drop in photocurrent not only because of the reduced surface area but also owing to the fact that photogenerated holes in bulk WO_3 have a mean diffusion length of 150 nm [34] before they recombine. When WO_3 particles of a less favorable surface/volume ratio are present, the probability that the holes reach the surface to react with water molecules is lower thus contributing to the reduced current density. This hypothesis is supported by the appearance of the curves in Fig. 7 which resemble more and more a straight line as the aging of the precursor is carried on, which is indicative of a higher electric resistance due to a less effective charge transport in the bulk.

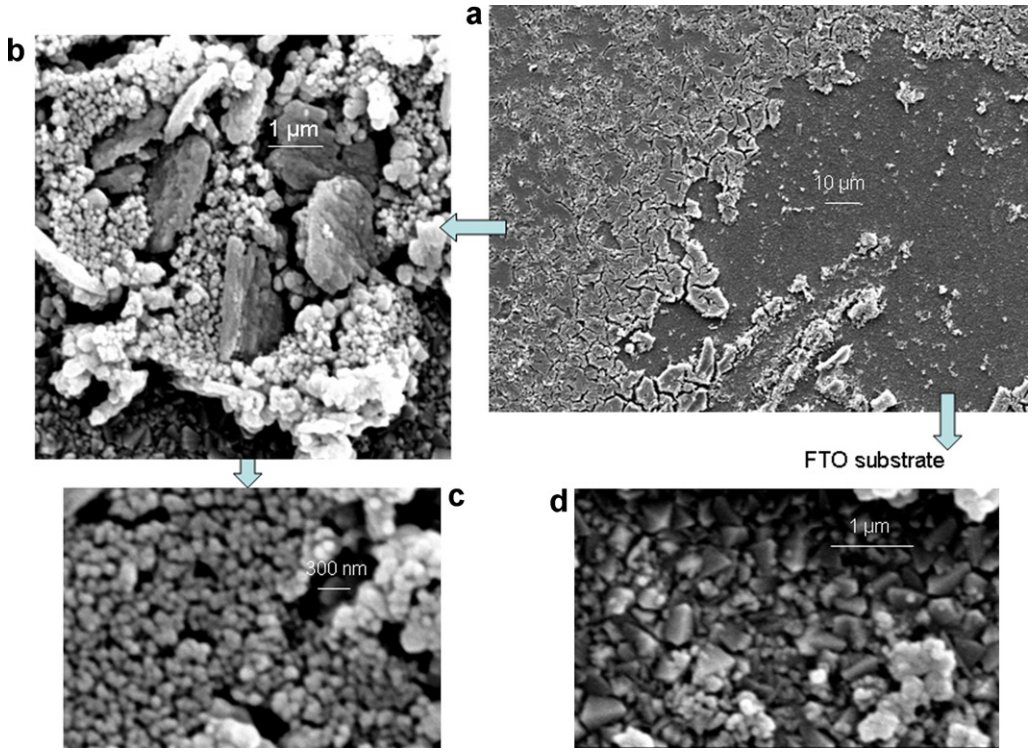

Fig. 9. SEM pictures of a photoanode obtained from a WO_3 suspension heated for 3 h at 60 °C. The conductive glass was glued to the aluminum stub. Magnification: (a) 23.65 k, (b) 50 k, (c) 85 k, (d) FTO substrate 23.65 k.

In order to further ascertain the surface area dependence of the photocurrent, the linear sweep cyclic voltammetry of the electrodes, upon which the J–V curves were measured, was recorded at the −0.2 to 0.5 V potential range in the dark (Fig. 8a). The voltammograms display a trend which strictly follows that observed for the corresponding J–V curves showing a diminution of peak current as the aging of the film precursor proceeds. The monitored process refers to the W(VI) → W(V) reduction and subsequent oxidation at the semiconductor particle surface, giving a maximum peak current for both waves which relates to the extension of the semiconductor liquid junction thus providing an indirect measure of the electroactive surface area. In Fig. 8b the integrated photocurrent density taken from J–V curves, integrated between 0.25 and 1.8 V, is plotted against the integrated cathodic peak area from CV giving a satisfactory linear correlation which further strengthens our conjecture.

It needs to be pointed out that a certain degree of variability in performance was observed within every batch of prepared photoelectrodes which did not show in all cases the regular trend reported here. This we attribute to the fact that after sintering, the deposited films often display a lack of uniformity as a result of cracks or missing parts as shown in Fig. 9a where the darkest uniform area visible on the right part of the SEM picture at 2k magnification is due to the underlying uncoated FTO. Although these films appear to be rather uniform at a macroscopic level, when they are observed under the electron microscope they show a fragmented structure consisting of a disjoint micron-sized domain made of particles of uniform size evenly distributed. In Fig. 9b and c different magnifications of one of these domains are presented belonging to a photoelectrode obtained after 3 h of aging (60 °C) of the precursor.

4. Conclusions

The controlled temperature aging of WO_3 suspensions, obtained via a simple sol–gel procedure, was found to produce nanoparticles of an increasing size. SdFFF and FlFFF were applied to obtain in a relatively short time size information on diluted aliquots of the colloid taken at regular intervals during the aging process. These separation techniques proved to be a convenient tool to assess the time evolution of these colloids providing together a satisfactory explanation for the particle size distribution in the suspensions. The obtained results seem to suggest that primary nanocrystals formed during the initial stage of WO_3 formation tend to change their shape spontaneously thus becoming well-defined square particles and to aggregate to form large clusters at a rate determined by the temperature set during the aging process. This conclusion was reached by observing that the d_s PSD curves initially increase in intensity and then shifts their maxima to more massive particles with a wider size distribution, while the d_h PSD curves show an almost constant particle amount of d_h ranging between 100 and 300 nm and an increasing post-analysis signal with the aging time.

In order to relate the particle size distribution of the suspensions to the photoelectrochemical properties of WO_3 in a biased photoelectrolytic cell, thin films were prepared on a transparent conductive substrate and tested. JV polarization curves in 1 M H_2SO_4 showed a progressive deterioration of photoelectrocatalytic performances with the aging of the film precursor. This behavior was mainly ascribed to the reduced electroactive surface area as suggested by the good correlation between JV photocurrents and the CV peak area related to W(VI) → W(V) process in the dark. The elucidation of the role of charge transport and electron–hole recombination as a function of WO_3 particle size in the films is currently under way.

Acknowledgements

This work was financially supported by the University of Ferrara (Fondo di Ateneo per la Ricerca Scientifica FAR 2009). The authors gratefully wish to thank Dott. Arrigo Aleotti for his assistance in performing SEM and TEM observations at the Centro di Microscopia Elettronica of the University of Ferrara.

The authors are also grateful to Dr. Maciej Zborowski and Dr. P. Stephen Williams of the Lerner Research Centre, Cleveland Clinic (Cleveland, OH) who kindly lent them their Flow FFF system and Microdyn-Nadir GmbH (Wiesbaden, Germany) for providing the membranes.

Appendix A. Supplementary data

Supplementary data associated with this article can be found, in the online version, at doi:10.1016/j.chroma.2010.11.061.

References

[1] N. Asim, S. Radiman, M.A. Bin Yarmo, Mater. Lett. 61 (2007) 2652.
[2] Y. Guo, X. Quan, N. Lu, H. Zhao, S. Chen, Environ. Sci. Technol. 41 (2007) 4422.
[3] M. Metikoš-Hukovic, Z. Grubac, J. Electroanal. Chem. 556 (2003) 167.
[4] H.T. Sun, C. Cantalini, L. Lozzi, M. Passacantando, S. Santucci, M. Pelino, Thin Solid Films 287 (1996) 258.
[5] E. Pelizzetti, Chemosphere 17 (1998) 499.
[6] J.S.E.M. Svensson, C.G. Granqvist, Sol. Energy Mater. 12 (1985) 391.
[7] C.G. Granqvist, Sol. Energy Mater. Sol. Cells 60 (2000) 201.
[8] C. Santato, J. Augustynski, M. Ulmann, M. Odziemkowski, J. Am. Chem. Soc. 123 (2001) 10639.
[9] H. Wang, T. Deutsch, J.A. Turner, J. Electrochem. Soc. 155 (2008) F91.
[10] H. Wang, T. Lindgren, J. He, A. Hagfeldt, S.E. Lindquist, J. Phys. Chem. B 104 (2000) 5686.
[11] S.S. Kalagi, D.S. Dalavi, R.C. Pawar, N.L. Tarwal, S.S. Mali, P.S. Patil, J. Alloys Compd. 493 (2010) 335.
[12] M. Gillet, A. Al-Mohammad, C. Lemire, Thin Solid Films 410 (2002) 194.
[13] A. Chemseddine, M. Henry, J. Livage, Rev. Chim. Miner. 21 (1984) 487.
[14] S.J. Hong, H. Jun, P.H. Borse, J.S. Lee, Int. J. Hydrogen Energy 34 (2009) 3234.
[15] M. Kozan, J. Thangala, R. Bogale, M.P. Mengüç, M.K. Sunkara, J. Nanopart. Res. 10 (2008) 599.
[16] J. Moore, E. Cerasoli, Particle Light Scattering Methods and Applications in Encyclopedia of Spectroscopy and Spectrometry, second ed., Elsevier, 2010, pp. 2077–2088.
[17] M.E. Schimpf, K.D. Caldwell, J.C. Giddings (Eds.), Field-Flow Fractionation Handbook, Wiley-Interscience, New York, 2000.
[18] F.V.D. Kammer, M. Baborowski, K. Friese, Anal. Chim. Acta 552 (2005) 166.
[19] P. Reschiglian, D.C. Rambaldi, A. Zattoni, Anal. Bioanal. Chem., doi:10.1007/s00216-010-4197-3.
[20] F. Angiuli, R. Argazzi, S. Caramori, C.A. Bignozzi, Patent WO2007/094019, A1.
[21] M. Sun, N. Xu, Y.W. Cao, J.N. Yao, E.G. Wang, J. Mater. Sci. Lett. 19 (2000) 1407.
[22] L. Meda, G. Tozzola, A. Tacca, G. Marra, S. Caramori, V. Cristino, C.A. Bignozzi, Solar Energy Mater. Solar Cells 94 (2010) 788.
[23] J.C. Giddings, Science 260 (1993) 1456.
[24] K.D. Caldwell, J.-T. Li, J.-M. Li, D.G. Dalgeish, J. Chromatogr. 604 (1992) 63.
[25] C. Contado, R. Argazzi, J. Chromatogr. A 1216 (2009) 9088.
[26] C. Contado, A. Pagnoni, Anal. Meth. 2 (2010) 1112.
[27] P.S. Williams, J.C. Giddings, Anal. Chem. 66 (1994) 4215.
[28] C. Contado, A. Dalpiaz, E. Leo, M. Zborowski, P.S. Williams, J. Chromatogr. A 1157 (2007) 321.
[29] C. Contado, A. Pagnoni, Anal. Chem. 80 (2008) 7594.
[30] Y.Y. Petrov, S.Y. Avvakumova, M.P. Siridova, L.E. Ermakova, O.M. Merkushev, Colloid J. 72 (2010) 663.
[31] M.J. O'Neil (Ed.), The Merck Index: An Encyclopedia of Chemicals, Drugs, and Biologicals, 14th ed., Merck Research Laboratories, Whitehouse Station, NJ, 2006.
[32] F. Shiba, M. Yokoyama, Y. Mita, T. Yamakawa, Y. Okawa, Mater. Lett. 61 (2007) 1778.
[33] A. Wolcott, T.R. Kuykendall, W. Chen, S. Chen, J.Z. Zhang, J. Phys. Chem. B 110 (2006) 25288.
[34] M.A. Butler, J. Appl. Phys. 48 (1977) 1914.